Biol. Cybern. 89, 170–178 (2003)
DOI 10.1007/s00422-003-0416-8

Biological Cybernetics

Parameter estimation in a model for multidimensional recording of neuronal data: a Gibbsian approximation approach

L. M. Ould Mohamed Abdallahi[1], **C. La Rota**[2], **M. Béguin**[3], **O. François**[4]

[1] Xerox Research Centre Europe, 6 Chemin de Maupertuis, F-38240 Meylan, France
[2] TIMC, Faculty of Medicine, F-38706 La Tronche, France
[3] LMC-IMAG, BP 53, F-38041 Grenoble, France
[4] TIMC, Faculty of Medicine, F-38706 La Tronche, France

Received: 8 November 2001 / Accepted: 25 March 2003 / Published online: 30 June 2003

Abstract. This article proposes improved numerical procedures for estimating parameters in a spatiotemporal lattice model introduced for the analysis of cortical activities monitored from arrays of diodes. The numerical algorithms are based on approximations inspired by statistical physics. Both Gibbsian and mean-field approximations are used; they allow for computing local conditional probabilities inside the lattice. The statistical procedures rely on the computation of pseudomaximum-likelihood estimators. The estimators are evaluated on the basis of Monte Carlo simulations. These simulations show that mean-field approximations are useful for reducing the variance of estimators when the data are recorded from arrays of 144 diodes (which are in accordance with standard practice). In light of these improved methods, we give new interpretations for a data set obtained from optical recording of a Guinea pig's auditory cortex in response to pure tone stimulations.

Key words: Multidimensional neuronal data – Interacting point processes – Gibbsian approximations – Mean-field approximations – Pseudomaximum likelihood – Auditory cortex

1 Introduction

Today several instrumentation techniques enable the recording of electrical activities inside the cortex during in vivo experiments using arrays of diodes (Grinvald et al. 1999; Stieglitz and Meyer 1999; Meyer et al. 2000; Takahashi et al. 2000). These techniques provide spatiotemporal data that are invaluable to the study of sensory information processing mechanisms inside the brain.

Correspondence to: O. François
(e-mail: Olivier.Francois@imag.fr)

Data provided by arrays of diodes are multidimensional. They contain endogenous randomness and exhibit spatiotemporal patterns that are supposed to reflect functional interactions between neurons or neuronal populations. Devising statistical methods to improve quantification and characterization of interactions is therefore a challenging issue.

In the late 1960s, Perkel et al. (1967) proposed a stochastic approach to the analysis of multiple spike trains based on point processes and crosscorrelation methods. Unfortunately, computing crosscorrelation statistics turns out to be difficult as the number of simultaneously recorded signals increases. As a consequence, this method is usually precluded in real-time processing of multidimensional recording. Following the pioneering approach of Little (1974), several statistical models of elementary interacting subcomponents inspired from those existing in statistical physics were introduced (Hervé et al. 1990; Martignon et al. 1995; Makarenko et al. 1997). Within this framework, multielectrode neuronal data were usually processed using Ising spin-like models. Yet computationally intensive Markov chain Monte Carlo methods are often necessary in order to implement these inference procedures. In addition, the resulting statistics may be difficult to interpret, as the meaning of the estimated parameters is not always clear from a biological point of view.

Recently, a different approach has been proposed by Francois et al. (2000). This approach is based on a model of interacting point processes, called the *diffusion model*, for which the parameters can be interpreted as frequencies of activation events. The data are assumed to be encoded as binary variables corresponding to the activities of populations of neurons (processing units) observed at the nodes of a two-dimensional grid. According to this model, the processing units become active according to some Poisson process (the innovation process). Activities at a given site may therefore diffuse and activate neighboring units according to a second Poisson process (the diffusion process).

Among the recent techniques, one of the most promising is optical recording using fluorescent

voltage-sensitive dyes. This technique consists of measurements of the emitted fluorescence changes related to the membrane potential fluctuations by means of an array of photodetectors. It enables in vivo observation of neural activities with high spatiotemporal resolutions. Since the measured signals mainly reflect the dendritic activities (Grinvald et al. 1988; Orback et al. 1996), this technique helps visualizing diffusions of synaptic potentials. However, the innovation process is usually extremely difficult to infer. In addition, even if one uses high resolutions, an intrinsic mixing of afferent and efferent activities is inevitable and makes difficult the direct interpretation of optical signals.

The approach developed in this article provides information about innovation and diffusion rates using the spatial distributions of activities at each instant of measure. The article is organized as follows. Section 2 describes the diffusion model mathematically. Section 3 presents improved numerical procedures for parameter estimation in this model. In the algorithms, Gibbsian approximations are performed at different stages of the computation of a pseudomaximum-likelihood estimator. The original method developed by Francois et al. (2000) was based on an indirect mean-field Gibbsian approximation (IMFGA). The new methods exploit the same idea in a more direct fashion and relax the assumption of pairwise interactions within the studied network. Numerical experiments based on simulations are reported in Sect. 4. In Sect. 5, we discuss a biological application. In a series of experiments held in Japan, Horikawa et al. (1996) collected in vivo optical recording of the Guinea pig's auditory cortex. They visualized the cortical excitatory and inhibitory functional organization of the focused area and studied the synaptic mechanisms. A subset of their data is used as an illustration of the way in which these statistical methods can be applied to a specific biological context.

2 The diffusion model

This section gives a mathematical description of the diffusion model as a model of interacting point processes. A set of n recording sites or diodes is denoted by S and is endowed with a lattice structure in two dimensions. For experimentalists, this array is usually regular, and $n = 12 \times 12 = 144$ is a typical number of recording sites. The neighborhood of a site i is the subset N_i of its four nearest sites.

Assume that n-dimensional binary matrices are recorded at each instant t according to a given sampling period and stored in a format similar to Table 1 of Francois et al. (2000) (p. 1834). Time is usually measured in milliseconds. The matrices are reindexed as *configurations*

$$x = (x_1, x_2, \ldots, x_{i-1}, x_i, x_{i+1}, \ldots, x_n) \ ,$$

that are viewed as realizations of Markovian spatiotemporal stochastic processes. Let (X_t) denote a sequence of such configurations. In a small interval of time $\mathrm{d}t$, we assume that at most a single site i changes its value. The resulting configuration is denoted as

$$x^i = (x_1, x_2, \ldots, x_{i-1}, 1 - x_i, x_{i+1}, \ldots, x_n) \ .$$

In the diffusion model, the probability of modifying the site i is computed as follows:

$$\mathbb{P}(X_{t+dt} = x^i \mid X_t = x) = q(x, x^i)\mathrm{d}t + o(\mathrm{d}t) \tag{1}$$

The transition rates $q(x, x^i)$ depend on three parameters λ, μ, and δ. We assume that

$$q(x, x^i) = \begin{cases} \delta & \text{if} \quad x_i = 1 \\ \lambda + \mu\bar{x}_i & \text{if} \quad x_i = 0 \ , \end{cases} \tag{2}$$

where $\bar{x}_i = \frac{1}{4}\sum_{j \in N_i} x_j$ is the local field at site i.

The three quantities λ, μ, δ are unknown parameters that vary with time. The parameter λ can be interpreted as the rate of arrival of external events (that typically consist of spikes or groups of spikes) according to some Poisson process. These external events generate activities in passive sites that become active. Then an active site may diffuse its activity toward a randomly chosen neighboring site at rate μ. The parameter μ encodes the intensity of such events. Finally, the duration of the activity in each site is an exponentially distributed random variable of mean $1/\delta$. Since the parameter δ can easily be estimated from the data, this study focuses on the estimation of λ and μ, and we denote the relationship as

$$\theta = (\lambda, \mu) \ .$$

3 Methods

This section presents four methods for estimating θ in the diffusion model. The first three methods are based on a pseudomaximum-likelihood approach and use Gibbsian approximations (GA). The last method is equivalent to a method of moments.

3.1 Pseudolikelihood

Owing to Besag (1974), the pseudolikelihood (PL) has become popular in estimating parameters for spatial binary models. Given the observation x, the pseudolikelihood method usually consists of maximizing the function defined as

$$PL(\theta) = \prod_{i=1}^{n} \mathbb{P}(X_i = x_i \mid X_j = x_j, \quad j \in N_i; \theta) \tag{3}$$

Let $u_i(\theta)$ denote the conditional probability for a site to be active given the states of its neighbors:

$$u_i(\theta) = \mathbb{P}(X_i = 1 \mid X_j = x_j, \quad j \in N_i; \theta)$$

Then, the PL function can be written as

$$PL(\theta) = \prod_{i=1}^{n} u_i(\theta)^{x_i}(1 - u_i(\theta))^{1-x_i}$$

3.2 Gibbsian approximations (GA)

Regarding the diffusion model, computing likelihoods or pseudolikelihoods is hardly feasible because the stationary distribution is not known analytically, and even the conditional probabilities $u_i(\theta)$ cannot be written explicitly.

Since no closed formulae are available, we use approximations. A first assumption is that the stationary distribution is a Markov Random Field (or Gibbsian distribution). We find the approximating distribution by supposing that the model is time-reversible. For time-reversible Markov processes, the transition rates and the stationary distribution $\pi_s(x)$ can be related as follows:

$$q(x,x^i)\pi_s(x) = q(x^i,x)\pi_s(x^i), \quad i \in S \tag{4}$$

According to Liggett (1985), this amounts to considering that the stationary distribution $\pi_s(x)$ is indeed Gibbsian.

Equation 4 allows computing the local conditional probabilities given the neighborhood. More specifically, we have

$$\pi_s(x_i|x_j, j \in N_i) = \frac{q(x^i,x)}{q(x^i,x)+q(x,x^i)} \tag{5}$$

and thus

$$u_i(\theta) \approx \frac{\lambda + \mu\bar{x}_i}{\delta + \lambda + \mu\bar{x}_i} \tag{6}$$

Finding the value $\hat{\theta}$ that maximizes the log criterion

$$\ell(\theta) = \log PL(\theta)$$

can be achieved from a standard iterative procedure

$$\theta_{k+1} = \theta_k - H^{-1}(\theta_k)\nabla\ell(\theta_k), \quad k \geq 0 \tag{7}$$

where $\theta_k = (\lambda_k, \mu_k)$ is the parameter at step k. Mathematical expressions for the gradient operator ∇ and the Hessian matrix H can be obtained from routine differential calculus.

3.3 Mean-field Gibbsian approximations (MFGA)

The second kind of approximation used in this work is called the *mean-field* approximation and is frequent in statistical physics. It assumes long-range weak connections and small correlations between sites inside the network. It is relevant here because the topology of interactions is usually unknown. Let us recall how this approximation applies. Francois et al. (2000) showed that

$$\lambda + (\delta + \lambda - \mu)\mathbb{E}[x_i] - \mu\mathbb{E}[x_i x_j] = 0, \quad j \in N_i \tag{8}$$

Estimating the expectation $\mathbb{E}[x_i]$ by the empirical value

$$\bar{u} = \frac{1}{n}\sum_{i=1}^{n} x_i \tag{9}$$

and using the mean-field approximation

$$\mathbb{E}[x_i x_j] \approx \bar{u}^2 \tag{10}$$

we obtain the so-called *mean-field equation*

$$\lambda + (\delta + \lambda - \mu)\bar{u} - \mu\bar{u}^2 = 0 \ . \tag{11}$$

The Mean-Field Gibbsian approximation (MFGA) estimation method is also based on the maximization of the pseudolikelihood criterion $\ell(\theta)$. The maximization is now performed under the mean-field constraint equation (Eq. 11). Using the mean-field constraint has the effect of linking λ to μ. Then a new criterion can be written in terms of a single parameter (we use μ) as follows:

$$\ell(\mu) = \sum_{i\,:\,x_i=1} \log\left(\frac{\delta\bar{u}}{1-\bar{u}} + \mu(\bar{x}_i - \bar{u})\right) - \sum_{i=1}^{n} \log\left(\delta + \frac{\delta\bar{u}}{1-\bar{u}} + \mu(\bar{x}_i - \bar{u})\right)$$

Again this criterion can be optimized using standard differential calculus and second-order procedures.

3.4 Indirect mean-field Gibbsian approximations (IMFGA)

The Indirect Mean-field Gibbsian approximation method introduced in Francois et al. (2000) required two steps. In the first step, it estimated the pseudomaximum likelihood parameters of the Ising model (the inverse temperature and the external field). Then it used mean-field approximations for finding the parameters λ and μ of the diffusion model from those of the Ising model. In contrast, the GA and MFGA methods compute the pseudolikelihood and the Gibbsian approximation at the same time.

The fundamental difference between IMFGA and GA/MFGA comes from the unknown order of the interactions present in the data. The pseudomaximum-likelihood method is strongly influenced by the assumptions made about these interactions. Because IMFGA is based on the Ising model, single-site and pair interactions prevail in this method. GA and MFGA make fewer assumptions about the true order of the interactions. Because mean-field statistics do not take the topology into account, the mean-field constraint plays the role of a regularizer with respect to the dependencies inside the array.

3.5 Moment method

In this section, we adopt an approach developed by Baddeley (1995) in a more general framework. Let ϕ be any test function defined on the set of configurations $\{0,1\}^S$. The generator of the Markov process is the operator Ω built as follows

$$\Omega\phi(x) = \sum_{i=1}^{n} q(x, x^i)\big(\phi(x^i) - \phi(x)\big), \quad x \in \{0,1\}^S \ . \quad (12)$$

Under stationarity, the theory of Markov processes tells that

$$\mathbb{E}[\Omega\phi(x)] = 0 \quad (13)$$

The idea developed by Baddeley (1995) is that clever choices of the test function ϕ can provide valuable methods for estimating the parameters of Ω. This would be achieved by solving the *unbiased equation*

$$\Omega\phi(x) = 0 \quad (14)$$

Baddeley (1995) uses this approach for estimating the parameters of a general probability distribution P. The method builds a Markov process that converges on P and then solves the unbiased equation. Clearly, the choice of ϕ is critical to the quality of the estimators. When P is a Gibbsian distribution, a natural choice for ϕ is the Hamiltonian associated with this distribution, and the approach coincides with the pseudolikelihood method.

In the present work, a specific couple of test functions ϕ_1 and ϕ_2 is utilized. These two functions are defined as the empirical spatial moments of order one and two. More specifically, we have

$$\phi_1(x) = \bar{u} = \frac{1}{n}\sum_{i=1}^{n} x_i \quad (15)$$

and

$$\phi_2(x) = \bar{r} = \frac{1}{n}\sum_{i=1}^{n} x_i \bar{x}_i \quad (16)$$

According to Eq. 14, estimators of θ are obtained by solving a linear system

$$A\theta^T = B \quad (17)$$

where A is the square matrix defined as

$$A = \begin{pmatrix} 1-\phi_1(x) & \phi_1(x)-\phi_2(x) \\ 2(\phi_1(x)-\phi_2(x)) & \sum_{i=1}^{n}\left[(1-x_i)\bar{x}_i^2 + x_i \sum_{j\in N_i}(1-x_j)\bar{x}_j/4\right]/n \end{pmatrix} \quad (18)$$

and B is the vector

$$B = \delta \begin{pmatrix} \phi_1(x) \\ 2\phi_2(x) \end{pmatrix} \quad (19)$$

With ϕ_1 and ϕ_2, the generator method coincides with the method of moments (MM) where the expected values $\mathbb{E}[x_i]$ and $\mathbb{E}[x_i x_j]$ are replaced by their empirical values in equation

$$2\lambda\mathbb{E}[x_i] - 2(\delta+\lambda)\mathbb{E}[x_i x_j] + 2\mu\mathbb{E}[\bar{x}_i(1-x_i)x_j] = 0 \ . \quad (20)$$

4 Validation of methods

This section reports experimental comparisons based on Monte Carlo simulations of the diffusion process.

4.1 Experimental design

In order to assess the statistical performances of the four estimators GA, MFGA, IMFGA, and MM, arrays of $30 \times 30 = 900$ sites have been simulated. As this number is not yet realistic with respect to experiments, arrays of 12×12 sites have been considered as well. One hundred Monte Carlo simulations have been run for each value of λ and μ starting from 0.0 to 2.0 according to a grid of mesh $h = 0.05$ (40,000 runs in all). Monte Carlo simulations were stopped when the equilibrium of the diffusion model was attained. Numerical maximization algorithms were stopped when the norm of the gradient was lower than 1.0e-4. In this section, the parameter δ is fixed to $\delta = 1.0$. Since it corresponds to the unit of time, its value does not influence the other estimators.

Two measures of performance are used. The first one is the mean square error (MSE), which is a standard measure in statistics. The *MSE* can be computed as

$$\mathrm{MSE}(\lambda,\mu) = \frac{1}{N}\sum_{k=1}^{N}\Big[(\bar{\lambda}_k - \lambda)^2 + (\bar{\mu}_k - \mu)^2\Big], \ \ N = 100$$

where $\bar{\lambda}_k$ and $\bar{\mu}_k$ represent the Monte Carlo estimates after the kth simulation. The second measure is called the *rate of success* and corresponds to the ratio of simulation runs for which the numerical procedure has converged.

4.2 Results

This section presents comparison results of the four estimation procedures. Recall that MFGA and IMFGA use mean-field approximations, whereas GA and MM do not. Figures 1–3 display the performances of Gibbsian approximation methods (GA, MFGA, and IMFGA) for 12×12 lattices (up) and 30×30 lattices (down). The results are presented as intensity maps that correspond to the levels of errors (left) and the rates of success of the numerical solver (right). Dark parameter areas indicate high statistical errors (MSEs increase from white to black). The rates of success range from less than 5% (black) to more than 95% (pale gray).

For 30×30 arrays, MSEs took similar values in all the Gibbsian approximation methods. Correct results are obtained except for parameters at the top corners in the figures. Because the top right corner corresponds to high values of mean activities, reliable estimates cannot

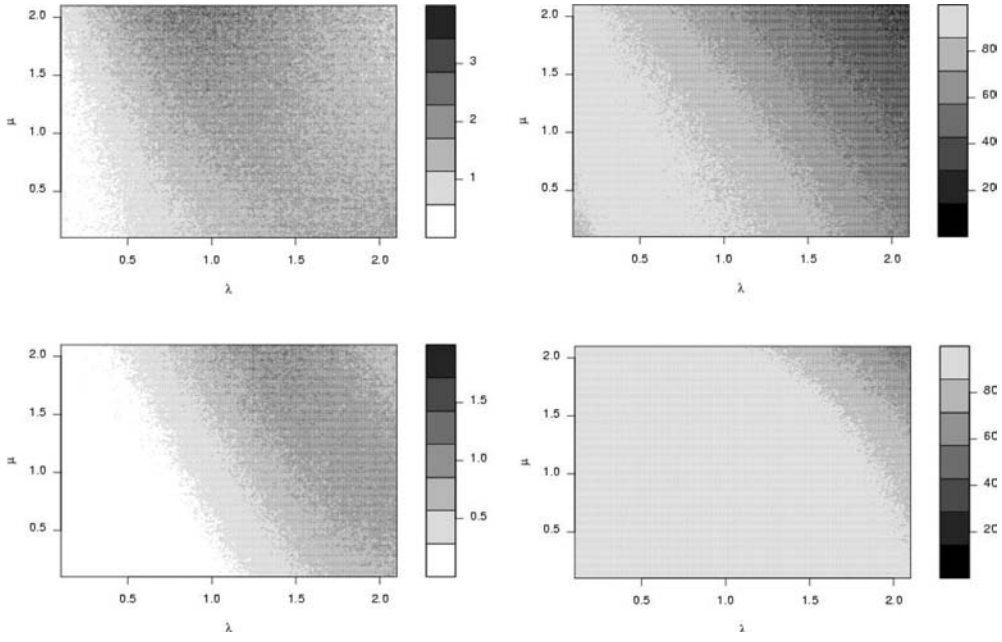

Fig. 1. Mean square errors (*left*) and rates of success (*right*) of the Gibbsian approximation method for lattices of 144 sites (*top*) and 900 sites (*bottom*)

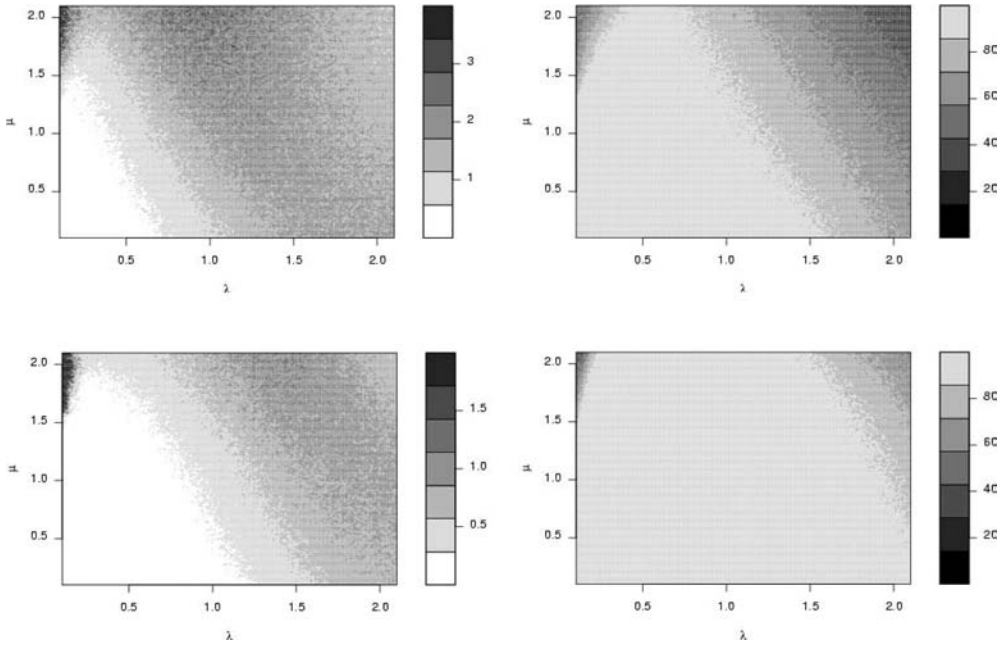

Fig. 2. Mean square errors (*left*) and rates of success (*right*) of the MFGA method for lattices of 144 sites (*top*) and 900 sites (*bottom*)

be obtained in this area (simulated binary patterns are almost saturated by 1s). The top left corner ($\lambda \ll 1$ and $\mu > 1.5$) corresponds to spatial covariances

$$c = \frac{1}{4n} \sum_{i;j \in N_i} x_i x_j - \bar{u}^2$$

that are large in absolute values ($|c| \geq 0.05$). In this area, the bias grows in both MFGA and IMFGA because mean-field approximations become erroneous. Overall, GA obtains the best rates of success and the smallest MSEs and can be considered as the best method for large arrays.

Figure 4 displays the performances of MM for 30×30 lattices. It also displays the value of the determinant of the linear system (Eq. 17). Small values of this determinant can be observed around a line of equation $\mu = 3 - 2\lambda$, and this shows that the method is unstable. MM appears to be correct for small values of λ and μ ($\lambda < 0.5$ and $\mu < 1.0$). However the quality of the estimators decreases significantly for $\lambda > 1$, and MM is globally beyond the other methods.

Regarding 12×12 lattices, the method that warrants the smallest MSEs and the highest rates of success is MFGA. (Because the performances were poor compared to the other methods, results of MM

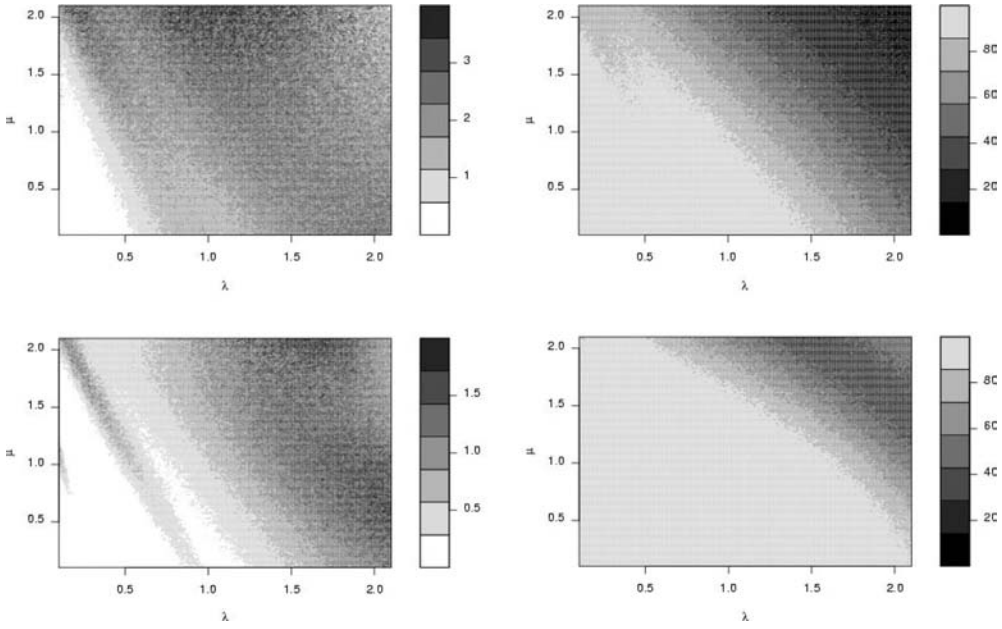

Fig. 3. Mean square errors (*left*) and rates of success (*right*) of the IMFGA method for lattices of 144 sites (*top*) and 900 sites (*bottom*)

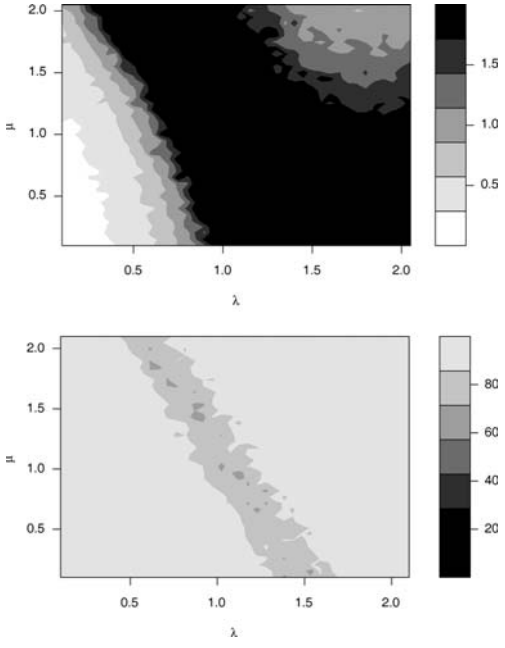

Fig. 4. Mean square errors (*top*) and determinants of the generator method (MM) with 30×30 sites

for 12×12 lattices were not presented). Surprisingly, IMFGA seems more reliable than GA. The rates of success are greater than 80% almost everywhere. This result is in favor of the mean-field approximation. It underlines that adding a mean-field constraint to the maximization procedure also regularizes the numerical algorithms. In addition, the biases introduced by these approximations are actually counterbalanced by significant gains in variances. To conclude, MFGA should be preferred as long as small arrays are used and small spatial covariances can be observed ($|c| \leq 0.05$).

5 Biological data

As an illustration of the way in which our statistical procedures can help analyze biological data, we reexamine a previously studied data set representing the electrical activity of the Guinea pig's auditory cortex (AC) in response to pure tone stimuli (Francois et al. (2000)). The format of data includes the preprocessing and the normalization of raw signals converted into binary data. Although these important steps may condition the interpretation of results, we assume that using binary variables instead of continuous signal variables helps in the understanding of qualitative behaviors and the spatial distribution of neural activities. We hence assume that such qualitative behaviors are correctly captured by the binary data.

During the experiment fluorescent signals emitted by the AC were monitored using a 12×12-channel photodiode array at a rate of 0.576 ms per frame (VSD optical imaging). The cortical recording area was 3 mm $\times$ 3 mm covering part of both the anterior (A, including the primary AC) and dorsocaudal (DC) fields. The measuring microscope was focused 200μ m below the surface of the AC (layers II/III). After contralateral ear stimulation with pure tones, transient excitatory responses followed by a long hyperpolarization were observed in fields A and DC. The raw data were converted into a sequence of 40 configurations. Further details about how the optical data were recorded can be found in Horikawa et al. (1996). The binary configurations have been processed using IMFGA by Francois et al. (2000).

Organization of the monitored area The AC is organized in column-shaped units that correspond to afferent thalamocortical and corticocortical projections and map sensory events onto the cortex. Columns are formed by many minicolumns linked together by horizontal

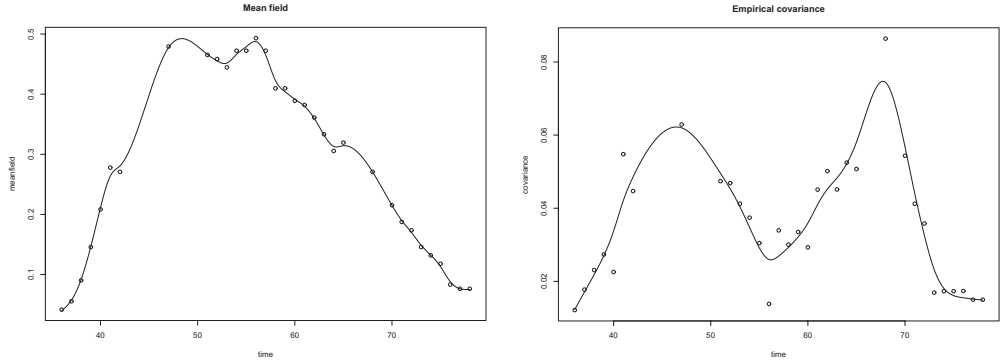

Fig. 5. Mean activities (*left*) and spatial covariances (*right*) estimated from the experimental dataset. The sampling period is 0.5 ms

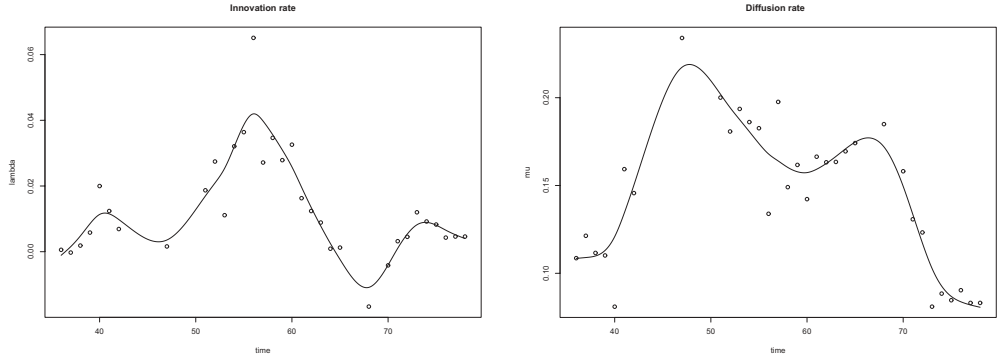

Fig. 6. Parameters λ (*left*) and μ (*right*) estimated from the experimental data set using the MFGA method

intracortical connections. Minicolumns have been identified as the basic ontogenetic information-processing units of the neocortex (Mountcastle 1997). In general, bundles of thalamic axons arriving at the cortex terminate in focal clusters situated in layers III and IV (Rockland 1998). In addition, evidence of a vertical flow of electrical activity from infragranular layers (V–VI) to supragranular layers (II–III) and of a horizontal diffusion at supragranular and infragranular layers has been obtained from neocortical slices (Kohn et al. 1997; Kubota et al. 1997; Kohn et al. 2000): neural activities propagate radially to superficial layers within columns and follow a minicolumn-related pattern dependent on the stimulus. Finally, distant functional cortical regions seem to be bounded by collateral axons from pyramidal neurons from layers III and V. These collateral axons run several millimeters joining cortical columns with similar functional properties (Ojima et al. 1991; Read et al. 2001).

Biological assumptions Optical recording techniques enable the study of in vivo cortical activities at mesoscopic scales below the cortical column size (300 μm) and even at minicolumnar scales (50 μm). Each site records the simultaneous activities of several minicolumns that may be part of different columns.

Our analysis will be based on the following assumptions. (1) Clusters of minicolumns are modular and interactive. At the fine mesoscopic scale, we assume diversity of neural responses among the modules. One can expect a relative homogeneity of receptive field properties at adjacent detectors but heterogeneity at distant detectors. (2) Fluctuations of electrical activities at this scale are supposed to reflect the coherent activities of local populations of neurons coding for specific combinations of stimuli features and receptive field properties. They are expected to exhibit complex waveforms due to nonlinear excitatory and inhibitory interactions within and among local minicolumns and are modulated by other activities (distant minicolumns, subcortical structures) (3) Most fluctuations contributing to VSDOI signals have their origin in excitatory synaptic activity occurring at the supragranular layers II and III. The observed signals are superpositions of afferent and intracortical activities (La Rota 2003).

Description of results Figure 5 displays the mean activities and the empirical spatial covariances measured from the binary data. Mean activities increase from 0% to 40%, reach a peak after 30 ms, and then decrease to 0. The spatial covariances are positive. Figure 6 displays the parameters λ and μ estimated thanks to the MFGA method. The shape of μ coincides with the shape of the spatial covariances. It indicates that this parameter actually measures a second-order interaction. In contrast, the shape of λ obtained with MFGA is different from the estimation obtained with IMFGA for which two "negative peaks" have been obtained. These negative peaks should be mostly considered as numerical artifacts.

6 Discussion

Previous studies of the fields A and DC of the Guinea-pig's AC in response to pure tones have revealed the existence of dynamical spatiotemporal patterns coding

for frequencies and intensities of sensory stimuli. These tonotopical patterns result from an asymmetrical spread of excitation in each field. They are shaped by the balance of excitatory postsynaptic activities mediated by the activation of both NMDA and non-NMDA receptors and inhibitory activities mediated by GABA receptors. They are also modulated by other sources such as the cholinergic system and the input activity from other cortical areas (Horikawa et al. 1996; Taniguchi et al. 1992; Taniguchi and Nasu 1993).

Horikawa et al. (1996) have shown the existence of excitatory responses mediated by non-NMDA receptors and have described their dynamics. These responses are localized in time and space. They start at focal points and diffuse along isofrequency bands in the rostrocaudal to ventrocaudal direction. These responses are followed after 10 ms by second ones, which last longer and have a larger amplitude but which are cancelled by a simultaneous GABAergic inhibition. Under normal conditions, the excitatory responses last 40–50 ms starting 17–20 ms after the stimulus onset. NMDA-receptor-mediated and GABAR responses start at 27–30 ms, i.e., 10 ms after the beginning of non-NMDA-receptor-mediated responses.

In this study, the curve of the spatial covariances suggests that the interactions between adjacent sites in the Guinea pig's AC are globally excitatory. For binary variables, positive spatial covariances actually indicate that the probability of coactivity at neighboring sites is greater than the value that would be obtained from independent superpositions of activities. We observe that the shape of covariances is closely related to the shape of the diffusion parameter μ. This result was expected and confirms the pairwise nature of interactions.

Direct measurements of input signals arriving at layers II–III of the AC are hardly feasible. Nevertheless, these input signals have their reflection in the parameter λ. The shape of the λ curve confirms the hypothesis that most inputs arriving at layers II–III are excitatory. The first peak of λ is correlated with the instants of arrival of afferent spikes from the MGB 14 ms after the stimulation (Rutkowski et al. (2000)) and coincides with the onset of the optical responses after 20 ms (Horikawa et al. 1996). The latency of the first peak of μ is correlated with the latency of GABAergic inhibition after 27 ms (Horikawa et al. 1996). These peaks are followed by oscillations of both λ and μ. The period of the oscillation is about 10 to 15 ms.

According to Mountcastle (1997), there are excitatory synaptic activities imposed via exhuberant recurrent collateral branches of pyramidal cell stem axons. These reentrant circuits create a bidirectional excitatory system: pyramidal cells of the supragranular layers innervate pyramidal cells of the infragranular layers and *vice versa*. In addition to this circuitry, pyramidal cells receive local inhibitory inputs from GABAergic interneurons. These interneurons receive the same afferent activities as the pyramidal cells (Horikawa et al. 1996; Metherate 1998). Therefore, the observed oscillations could result from the positive feedback between infragranular and supragranular layers. In addition, the duration of the GABAergic inhibition could be responsible for the distance between the two peaks.

The above conjectures must be weighted by the following facts. (1) The analysis might be sensitive to the preprocessing of continuous signals. (2) The signals have been obtained with the RH795 fluorescent dye, which is contaminated by a large amount of noise. (3) The nature and the intensity of anaesthesia (barbiturates) may condition the results of the experiments. The interpretation of data needs more evidence under different experimental conditions, e.g., awake animals (La Rota 2003). (4) We assume homogeneous structures. In the primary AC, the modules follow a band pattern arrangement related to sound frequencies (isofrequency band). In addition, there is a single tonotopic map in the medial geniculate ventral nucleus, which splits when projected onto the cortex in the two adjacent tonotopic fields A and DC (Redies et al. 1989a, b). The A and DC areas of the AC cannot be considered as fully homogeneous.

Nevertheless, we believe that binary variables are able to capture the rough patterns of spatiotemporal information inside the cortex and that such data are robust in this respect. Continuous variables might be useful for detecting further details of temporal activities. However, their analysis remains difficult at this time. The above data set from the guinea pig's AC is a typical example of how spatial statistical methods could be applied in processing complex neural signals.

Acknowledgements. The authors would like to thank the French national project ACI Télémédecine "Propriétés Emergentes Fonctionnelles et Modèles non-linéaires" for its support.

References

Baddeley AJ (1995) Time invariance estimating equations. Technical Report 22, Department of Mathematics, University of Western Australia

Besag JE (1974) Spatial interaction and the statistical analysis of lattice systems. J R Statist Soc B 60: 172–236

Francois O, Mohamed Abdallahi L, Horikawa J, Taniguchi I, Hervé T (2000) Statistical procedures for spatiotemporal neuronal data with applications to optical recording of the auditory cortex. Neural Computat 12: 1821–1838

Grinvald A, Frostig RD, Lieke E, Hildesheim R (1988) Optical imaging of neuronal activity. Physiol Rev 68: 1285–1366

Grinvald A, Shoham D, Shmuel A, Glaser D, Vanzetta I, Shtoyerman E, Slovin H, Sterkin A, Wijnbergen C, Hildesheim R, Arieli A (1999) In-vivo optical imaging of cortical architecture and dynamics. In: Windhorst U, Johansson H (eds) Modern techniques in neuroscience research, Springer, Berlin Heidelberg New York, pp 893–969

Hervé T, Dolmazon JM, Demongeot J (1990) Random field and neural information. Proc Natl Acad Sci USA 87: 806–810

Horikawa J, Hosokawa Y, Kubota M, Nasu M, Taniguchi I (1996) Optical imaging of spatiotemporal patterns of glutamatergic excitation and gabaergic inhibition in the guinea-pig auditory cortex. J Computat Physiol 497: 629–638

Kohn A, Metz C, Quibrera M, Tommerdhal MA, Whitsel BL (2000) Functional neocortical microcircuitry demonstrated

with intrinsic signal optical imaging in vivo. Neuroscience 95: 51–62
Kohn A, Pinheiro A, Tommerdhal MA, Whitsel BL (1997) Optical imaging in vitro provides evidence for the minicolumnar nature of cortical response. Neuroreport 8: 3513–3518
Kubota M, Sugimoto S, Horikawa J, Nasu M, Taniguchi I (1997) Optical imaging of dynamic horizontal spread of excitation in rat auditory cortex slices. Neurosci Lett 237: 77–80
La Rota C (2003) Analyse de l'activité électrique multisite du cortex auditif chez le cobaye. PhD manuscript, Université Joseph Fourier, Grenoble, France
Liggett TM (1985) Interacting particle systems. Springer, Berlin Heidelberg New York
Little WA (1974) Persistent states in the brain. Math Biosci 19: 101–114
Makarenko VI, Welsh JP, Lang EJ, Llinas R (1997) A new approach to the analysis of multidimensional neuronal activity: Markov random fields. Neural Netw 10: 785–789
Martignon L, Von Hasseln H, Gruen S, Aertsen A, Palm G (1995) Detecting higher-order interactions among the spiking events in a group of neurons. Biol Cybern 73: 69–81
Metherate R (1998) Synaptic mechanisms in auditory cortex function. Front Biosci 3: d494–501
Meyer JU, Schüttler M, Thielecke H, Stieglitz T (2000) Biomedical microdevices for neural interfaces. Proceedings of the 1st annual international IEEE-EMBS special topic conference on microtechnologies in medicine and biology, Lyon, France, 12–14 October 2000, pp 447–452
Mountcastle VB (1997) The columnar organization of the neocortex. Brain 120: 701–722
Ojima H, Honda CN, Jones EG (1991) Patterns of axon collateralization of identified supragranular pyramidal neurons in the cat auditory cortex. Cereb Cortex 1: 80–94
Orback HS, Cohen LB, Grinvald A (1996) Optical monitoring of optical activity in the mammalian sensory cortex. J Neurosci 5: 1886–1895
Perkel DH, Gerstein GL, Moore GP (1967) Neuronal spike trains and stochastic point processes. II. simultaneous spike trains. Biophys J 7: 419–440
Read HL, Winer JA, Schreiner CE (2001) Modular organization of intrinsic connections associated with spectral tuning in the cat auditory cortex. Proc Natl Acad Sci USA 98: 8042–8047
Redies H, Brandner S, Creutzfeld OD (1989a) Anatomy of the auditory thalamocortical system of the guinea pig. J Comp Neurol 282: 489–511
Redies H, Sieben U, Creutzfeld OD (1989b) Functional subdivisions in the auditory cortex of the guinea pig. J Comp Neurol 282: 473–488
Rockland KS (1998) Complex microstructures of sensory cortical connections. Curr Opin Neurobiol 8: 545–551
Rutkowski RG, Wallace MN, Shackleton TM, Palmer AR (2000) Organisation of binaural interactions in the primary and dorsocaudal fields of the guinea pig auditory cortex. Hearing Res 145: 177–189
Stieglitz T, Meyer JU (1999) Microtechnical interfaces to neurons. In: Manz A, Becker H (eds) Microsystem technology in chemistry and life sciences. Springer, Berlin Heidelberg New York, pp 131–162
Takahashi H, Ejiri T, Nakao M, Matsumoto K, Mase F, Hatamura Y, Hervé T (2000) Multipoint microelectrode for direct recording of auditory evoked potentials on the auditory cortex of a rat. Proceedings of the 1st annual international IEEE-EMBS special topic conference on microtechnologies in medicine and biology, Lyon, France, 12–14 October 2000, pp 512–517
Taniguchi I, Horikawa J, Moriyama T, Nasu M (1992) Spatiotemporal pattern of frequency representation in the guinea pig auditory cortex. Neurosci Lett 146: 37–40
Taniguchi I, Nasu M (1993) Spatio-temporal pattern of sound intensity in the guinea pig auditory cortex observed by optical recording. Neurosci Lett 151: 178–181